Biointerface Research in Applied Chemistry
Open-Access Journal (ISSN: 2069-5837)

Article
Volume 13, Issue 5, 2023, 447
https://doi.org/10.33263/BRIAC135.447

Coordination Polymer Based on Phenazine Ligands and Silver with Two-Dimensional Organization and High Conductivity

Irina Sapurina[1], Mikhail A. Shishov [1,2], Anna E. Bursian [1], Mikhail E. Kompan [3], Vladislav G. Malyshkin [3], Nadezda Pizurova [4]

[1] Institute of Macromolecular Compounds, Russian Academy of Sciences, St. Petersburg 199004, Russian Federation
[2] Peter the Great St. Petersburg Polytechnic University, ul. Politekhnicheskaya 29, 195251 St. Petersburg, Russian Federation
[3] Joffe Physico-Technical Institute, Russian Academy of Sciences, St. Petersburg, 194021 Russia
[4] Institute of Physics of Materials, Czech Academy of Sciences, 616 62, Brno, Czech Republic
* Correspondence: sapurina@mail.ru (S.I.);

Scopus Author ID 6602755296
Received: 3.07.2022; Accepted: 7.08.2022; Published: 21.12.2022

Abstract: A novel coordination polymer from phenazine ligands and silver was synthesized using a one-pot method. A distinctive feature of this synthetic approach is that phenazine was produced at the beginning of the process by oxidative aniline dimerization; then, phenazine ligands and an excess of silver nitrate participated in self-assembly to form a planar crystalline organometallic structure. The composition and morphology of the product were determined by chemical analysis, electron spectroscopy, X-ray diffraction, scanning electron microscopy, and transmission electron microscopy. It was demonstrated that the coordination polymer has a layered graphene-like structure. The specific electrical conductivity of the material exceeds 1000 S/cm, which can be explained by the presence of silver metal in the polymer. Silver metal is generated during the oxidation of aniline in stoichiometric amounts and, as a guest element, is localized on the surface of polymer sheets in the form of nano-deposits. All product components are biocompatible, contain silver in both metallic and ionic states, and can serve as an alternative to the Ag/AgCl electrodes commonly used for encephalography.

Keywords: coordination polymer; phenazine; two-dimensional structure; conductivity.

1. Introduction

Coordination polymers (CP) are hybrid organometallic compounds in which organic ligands are combined with transition metal atoms/ions to form complex spatial architectures [1,2] Metal-organic frameworks can have different spatial structures: three-dimensional, two-dimensional (2D), and one-dimensional. Moreover, a metal-organic network can demonstrate crystallinity and simultaneously have a large specific surface area [2]. The factors promoting the appearance of the crystalline structure are the presence of repeating organic fragments (ligands), which are similarly linked to each other at the expense of interaction with a metal, and the regular spatial arrangement of such fragments (Figure 1). According to the BET analysis, such materials' specific surface area values vary from tens to hundreds of m^2/g; in some cases, they can exceed 1000 m^2/g [3]. Furthermore, since coordination polymers contain significant free interatomic spaces, they can incorporate not only individual atoms but also their clusters and even small molecules [4].

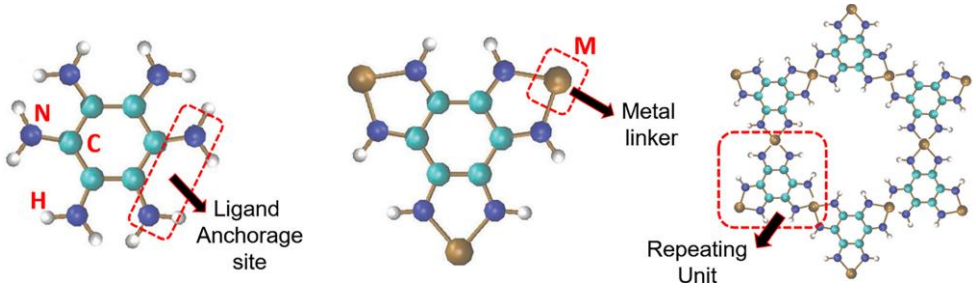

Figure 1. Scheme of assembly of ligand-metal fragments. Reproduced from Ref. [1].

Various organic ligands are used in the synthesis of CP; as a rule, these are highly stable aromatic compounds with conjugated π - electronic systems (substituted triphenylamines, phenylenediimine, porphyrins, tetrathiafulvalene, phthalocyanines, etc.) [5,6]. The ligands contain various functional groups (carboxylate, pyridine, azole, thiol, amino structures, etc.), which include electron donor atoms (O, N, S). Electron donor atoms interact with a transition metal due to the bonding between their p-orbitals and d-orbitals of the metal. It is believed that, in addition to the p-d electronic interaction, a significant contribution to the bonding can be made by the π-π and π-d electronic interactions, in which the π-electronic structure of the ligand takes part [6,7]. Thus, spatial architecture and properties of a CP are determined by the rigidity of the used aromatic ligand, ligand size, nature of the linking metal, and its location.

The properties and possible practical applications of CPs are as diverse as their structures. The presence of catalytically active transition metals provides the activity of these materials in catalysis [8,9]. Due to high permeability and large free volume, CP is used as a sorbent [10]. The possibility of intercalation-deintercalation of large ions is exploited in developing new power sources [11,12]. Electrical conductivity and satisfactory charge carrier mobility inherent to coordination polymers enable one to use them in field-effect transistors [13, 14]. New optoelectronic devices with the possibility of emission control are based on various CPs with intense luminescence. [15,16]. Many new sensors have been developed in which CP acts as detecting materials [17,18].

Many CPs exhibit paramagnetism and may be of interest to spintronics [19]. Theoretical studies predict the possibility of the appearance of ferro- and ferrimagnetic CP [5,13,19-22]. In addition, the introduction of the so-called "guest elements" into the free space of the CP matrix has a significant effect on the properties of materials and expands the possibilities of their practical use. Thus, lanthanide ions (Eu^{3+}), which demonstrate intense luminescence, have been introduced into the CP containing luminescent ligands; this combination has made it possible to create the material with emission wavelengths covering the region from ultraviolet to near-infrared [23].

The CP with biosafety and biocompatible properties are of great interest for biomedical and medical applications [24-26]. They are used as detection materials of biosensors [27], as drug carriers and drug delivery systems [28-30], and as fluorescence tags for the diagnosis of various diseases, including cancer [31-33]. The antimicrobial activity of CP against widespread pathogens and fungal cell inactivation ability is intensively studied [34-39]. The possibility of using CP for cancer treatment is being studied [40-42].

Electrical conductivity is one of the most important and practically significant characteristics of CP. For the currently known CP, this parameter varies over a very wide range (from 10^{-14} S/cm to 10^{3} S/cm, i.e., covers 17 orders of magnitude) [3]. Most CP are dielectrics and semiconductors with conductivity values not exceeding 10^{-5} S/cm. However, several authors have obtained the CP that demonstrated a nonzero state density at the Fermi level and

thus could be classified as metals [43]. The main way to increase the conductivity of a metal-organic framework is the introduction of guest elements with pronounced electrical conductivity. These are metals, their clusters, and conducting polymers that create percolation of transport routes through the material [4]. It is believed that a matrix containing a conjugation system can also participate in the transport of charge carriers [1].

The presence of redox-active metals at matrix sites can also contribute to transport by increasing the number of charge carriers. The CPs with conductivity values higher than 10^{-2} S/cm are considered highly conductive [3,44]. Among the known CPs, the highest conductivity (1500 S/cm) was found for the coordination polymer based on benzenehexathiol ligand and copper. This material is obtained in the form of a film on the interface of two immiscible solvents [44].

CPs with two-dimensional (2D) morphologies are of particular interest, characterized by considerable spatial inhomogeneity. This is caused by the existence of strong covalent bonds between atoms in the lateral direction and weak van der Waals interaction between the planes [45,46]. This should lead to significant anisotropy of material properties. Coordination polymers with a small number of layers and, in the limit, single-layer 2D polymers can have nontrivial electronic properties and demonstrate quantum effects with the appearance of unusual conducting, optical, and magnetic characteristics [1,47].

This work reports the one-pot synthesis of a new CP based on phenazine ligands (Phz) and silver (Ag). The synthesis involved the preparation of phenazine by oxidative dimerization of aniline under the action of silver nitrate and the subsequent release of metal nanoparticles. In the end, the self-assembly of phenazine ligands into a crystalline metal-organic framework occurred due to interaction with excess $AgNO_3$. In the Phz-Ag composition, silver performs two functions: silver ions serve as binding elements for the ligands, while the silver metal clusters play the guest elements responsible for the high conductivity of the material. The Phz-Ag polymer has a low-layer 2D organization; its conductivity exceeds 1000 S/cm. Both components of CP: phenazine ligand and silver, are biocompatible and widely used in medicine [48-52]. Considering the biosafety of the material and its high electrical conductivity, we can predict the use of CP as a bioelectrode intended for contact with human skin.

2. Materials and Methods

Synthesis of the CP based on phenazine ligands and silver was carried out in an aqueous-organic medium (H_2O/isopropanol: 5/1) using aniline (0.1 M) as a precursor of phenazine and silver nitrate (the molar ratio between components varied from 1/2.5 to 1/3.5). Initially, the reagents were completely dissolved. Then, the reaction proceeded in the solution under normal conditions; the air was constantly bubbled through the reaction medium. The CP was obtained in the form of suspension that occupied the volume of the reaction medium. The final product was isolated by filtration, washed with water, and dried under ambient conditions; the dried product was a yellow-brown powder.

The silver content was determined by burning the organic component of the sample at temperatures above 600°C in the air since silver is not oxidized by oxygen even at high temperatures. Elemental analysis of the organic component (C, H, N) was performed using a VARIO EL III Elemental Analyzer (Elementar, Germany). The oxygen content was calculated as a residue.

The sample structure was investigated with the aid of a JEOL JEM 2000FX and a Carl Zeiss Supra 55 VP electron microscope. Photoelectron X-ray spectroscopy was performed

using standards (C, N, O, Ag); the instrument's sensitivities to these standards were equal to 0.62, 0.11, 0.23, and 0.76, respectively.

Electronic absorption spectra were obtained using an SF-256 UV-vis spectrometer (LOMO-Photonics) in the 200 – 1200 nm wavelength range. Samples (Phz-Ag, $AgNO_3$) were dispersed in water. The electronic spectrum of phenazine was obtained in ethanol (due to its insolubility in water); polyaniline dispersion was studied in aqueous media at different pH values. The oxidized form of phenazine was produced by oxidation with $AgNO_3$; the spectrum was obtained in the aqueous medium.

Conductivity was measured by the four-point van der Pauw method using a Keithley 237 power source and a Keithley 2010 Multimeter-Voltmeter; the samples were compressed into pellets using a manual hydraulic press at a pressure of 600 MPa. Measurements were carried out at room temperature.

The morphology of the products was investigated using a High-Resolution Transmission Electron Microscopy (HRTEM, JEOL JEM-2100F, with a 200kV field emission).

3. Results and Discussion

3.1. Synthetic strategy for CP and its implementation.

The top-down approach that involves crushing materials in preparing coordination polymers is rarely used. As a rule, CPs are synthesized using the bottom-up technology based on the self-organization processes of atoms, ions, and molecules. Organic ligands and transition metal compounds are used as starting reagents. The electron donor atoms of a ligand interact with the atoms/ions of a d-metal to form π-d orbitals. The resulting mobile fragments adjust to each other, forming the organized organometallic structure. The synthesis can be performed at the solid/liquid, liquid/ liquid, and solid/gaseous interfaces or in solution [53-55]. Synthesis in solution is considered the most promising technique since it is simple and allows one to obtain large quantities of CP [1]. The necessary conditions for successful CP assembly are the mobility of reagents and the absence of molecular aggregation. However, there is a serious technical problem related to the fact that large organic ligands (such as porphyrins, tetrathiafulvalene, phthalocyanines, etc.) are expensive, poorly soluble, and not readily available. Besides, the solvent for a transition metal compound rarely coincides with the solvent for a ligand [6]. In our opinion, one of the solutions to this problem is to "start" the synthesis of CP using simpler and more readily soluble organic molecules, which serve as precursors of the selected organic ligands.

One of the synthetic pathways for large aromatic ligands is the oxidative activation of the aromatic ring's C–H bond that provides the possibility of attaching a new functional group [56-58]. Several recent studies have shown that silver compounds can be involved in functionalizing a wide range of arenes with electron-donor and electron-withdrawing properties. Silver salts taken in stoichiometric amounts with respect to an arene provoke oxidative activation of the arene C–H bond. As a result, the arene is bound to the new group at C – C and/or C – heteroatom bonds, and the aryl derivative is enlarged [59]. The formation of silver metal nanoparticles accompanies the reaction. Oxidative C–H functionalization catalyzed by transition metal salts is considered a new synthesis technology [60-62]. This technology has been used to develop new reactions, such as trifluoromethylation [56] and phosphorylation of aromatic molecules [54], C – H arylation/alkylation of quinones [58],

dimerization/cyclization of aryl-substituted amines [56]. However, the mechanisms of these processes are not well understood.

To obtain the phenazine ligand, we used a new synthetic method for phenazine involving the dimerization of aniline under the action of silver salt [56]. This approach made it possible to overcome the problem of poor solubility of the phenazine heterocycle. The authors of [56] have shown that aniline's ortho C–H bond is activated under the action of Ag^+ complexes combined with oxidizing agents (palladium salts, persulfates, oxygen). The authors [56] believe that the C–H activation and formation of two new C–N bonds leading to the appearance of phenazine heterocycle occur synchronously and require the participation of two aniline molecules. According to the terminology of the authors, this is the "amination cyclization-oxidation cascade" reaction [56] (Figure 2).

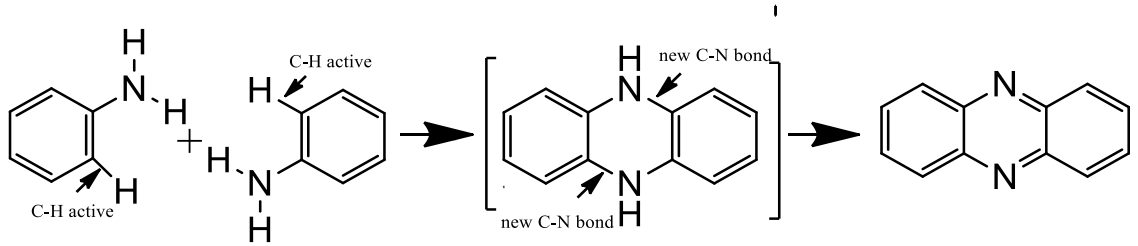

Figure 2. Scheme of phenazine synthesis by oxidative activation of the C-H bond of aniline under the action of Ag^+ (oxidative cascade cyclization of aniline). Dihydrophenazine is formed as an intermediate product of the synthesis.

Using a wide range of aniline derivatives, it has been shown that the formation of phenazine under the action of Ag^+ and 1% Pd salt as a cocatalyst proceeds rapidly and with high yields. In the case of unsubstituted aniline, the phenazine yield reaches 87%, and aniline azo-dimer (10%) is formed as a by-product [56]. In the absence of a palladium catalyst, the same reaction proceeds much more slowly. Phenazine formed in the reaction medium can participate in further transformations, for example, in the process of CP assembly with the participation of a transition metal salt. During the phenazine synthesis, a stoichiometry is observed between the amount of oxidized aniline and reduced silver. In the synthesis products, silver metal particles (Ag 20-40 nm) [56] were detected by X-ray photoelectron spectroscopy. In our opinion, the appearance of reduced silver made it possible to solve the problem of introducing a guest element into the CP.

Based on this information, we were able to develop a strategy for the one-pot preparation of CP with the simultaneous introduction of silver nanoparticles into the polymer. The synthesis proceeded in the solution and began with the oxidative dimerization of aniline (An) under the action of $AgNO_3$ with the formation of one phenazine molecule and two atoms of reduced silver. The processes of self-organization of the products proceeded in parallel with this reaction and included the binding of poorly soluble phenazine ligands with excess $AgNO_3$ (formation of the CP), and saturation of the CP with the guest element in the form of silver metal nanostructures.

$$2An + 2Ag^+ \rightarrow Phz + 2Ag$$

$$Phz + AgNO_3 \rightarrow CP\ (Phz\text{-}Ag)$$

Synthesis of the CP based on phenazine ligands and silver was carried out in the volume of an aqueous-organic phase using inexpensively available reagents (aniline and silver nitrate). According to [56,58], a saturation of the aqueous phase with oxygen increases the phenazine yield since the presence of additional oxygen facilitates oxidation of the dihydrophenazine intermediate to phenazine. The reaction medium became cloudy with time, and the content of

the yellow-brown suspension increased. Visible agglomerates precipitated on the bottom and walls of the flask. After two weeks, the yield of coordination polymer was 30-35% with respect to the weight of the initial reagents. The resulting product could be readily redispersed in water, where it formed a stable colloid. The product formed the film with a gold metallic sheen at the water/air interface and upon sorption on a smooth surface (Figure 3).

Figure 3. Phz-Ag film at the water-air interface.

3.2. Composition of the product.

The product's chemical composition was determined using elemental analysis (C, N, H content), and the content of silver in Phz-Ag was estimated by burning the organic component of the sample at temperatures above 600°C in air. The silver content in the synthesis products is 63-65 wt.%, corresponding to approximately 3.5 Ag atoms with respect to the molar fraction of the organic part. It should be noted that the burning method does not answer the question of whether the composite contains silver in ionic or metallic form since ionic silver at temperatures above 600°C also turns into silver metal. Therefore, the content of 63-65 wt.% may correspond to the presence of silver in both metallic and ionic forms.

The organic constituent of the product was isolated by dissolving CP in hot ethanol using a Soxhlet apparatus. Its elemental composition was determined after drying. It turned out that the composition of the organic part (carbon 60-63%, nitrogen 12-14%, hydrogen 3-4%, and oxygen residue 19-20%) coincided well with the formula of the oxidized phenazine molecule (C 60%, N 13%, H 3.3%, O 19.8%) containing NO_3 group as a counterion. The density of the resulting composite compressed into a pellet under a pressure of 100 MPa was equal to 2.2 g/cm^3. This is slightly lower than the theoretical density (2.5 g/cm^3) calculated from the density of silver (10.5 g/cm^3, theoretical content 63 wt.%) and the density of phenazine (1.2 g/cm^3, theoretical content 37 wt.%).

Per the stoichiometry of the redox process involving aniline and silver ions, the oxidation of two aniline molecules to obtain one phenazine molecule should consume two $AgNO_3$ molecules and give two atoms of reduced metal. Another 0.5 Ag^+ atom can be reduced to metal due to the oxidation of one of the nitrogen atoms of each phenazine ring. In total, we obtain 2.5 silver atoms per phenazine molecule. At the same time, the mass fraction of silver in the composite is higher and amounts to 3.5 Ag atoms per phenazine molecule, which can be explained by the presence of ionic silver in the composite. The presence of ionic silver in the sample is confirmed by the appearance of the 295 nm band in the electronic absorption

spectrum of Phz-Ag, which is characteristic of the spectrum of silver nitrate in water (Fig. 8). The indirect confirmation of the presence of ionic silver was also obtained by X-ray photoelectron spectroscopy. Thus, it was possible to estimate the approximate contribution of silver metal, which turned out to be lower than the total silver content in the material. Thus, on the basis of the obtained results, the product formula can be represented as [$Ag_{3.5}$ (Phz^{+} NO_3^{-})], where silver is contained partially in the metallic form and partially in the ionic state.

3.3. Morphology of the material.

Figures 4 - 6. show electron microscopy images of the obtained product. The SEM studies (Fig. 4 a) revealed the particles in the form of thin two-dimensional plates with lateral sizes of 5 - 8 microns. Judging by the size of the end face and the transparency of the particles, it can be calculated that the thickness of such a plate does not exceed 5-10 nanometers. This value indicates that the particles consist of only several polymer layers. With an increase in the accelerating voltage of the electron beam (Figure 4b), silver nanoparticles (light objects) localized on polymer planes become distinguishable. Ag particles are arranged in rows framing the edge of the polymer plates. Most Ag particles are tens of nanometers in size, but there are also larger crystals (several hundred nanometers in size). The polymer plates are heterogeneous (motley color) and frequently have triangular shapes.

The transmission electron microscopy image (Figure 5a) reveals distinguished dark silver nanoparticles on the periphery of the plate; the pattern of stripes on the plane of the polymer particles can be seen (which was visualized in Figure 4b as a "motley color"). These dark stripes correspond to silver metal. The uneven distribution of the metal over the surface is possibly caused by the dipole-dipole attraction between neutral silver atoms (van der Waals interaction) [63].

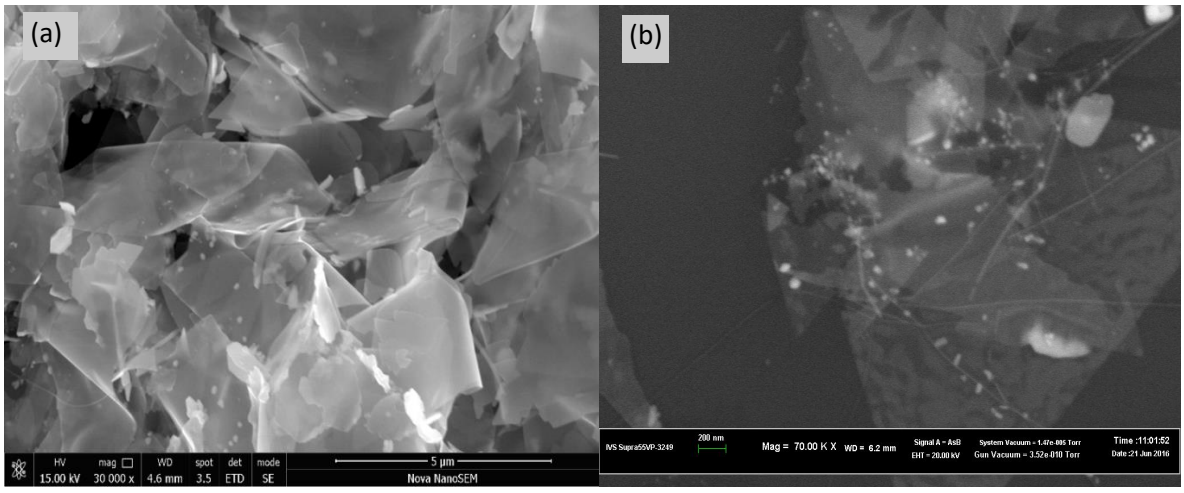

Figure 4. SEM images of the Phz-Ag sample: (**a**) the image obtained at standard measurement parameters; (**b**) the image taken at the maximum accelerating voltage of the electron beam.

Figure 5 (a) presents a TEM image of two superimposed particles (the large (foreground) object is shown in the lower right corner of the picture; the small (background) object can be seen in the upper part of the image). The micrograph gives an insight into the initial stage of the nucleation of microcrystals. The edge of the larger particle is a partially rounded polyline. The particle began to acquire a hexagonal shape in accordance with the symmetry of the aromatic rings (120 ° angle) from which it was formed. The smaller particle retains a rounded shape with a smaller boundary length; this observation can be explained by the necessity of minimizing thermodynamic losses related to excess energy of boundaries.

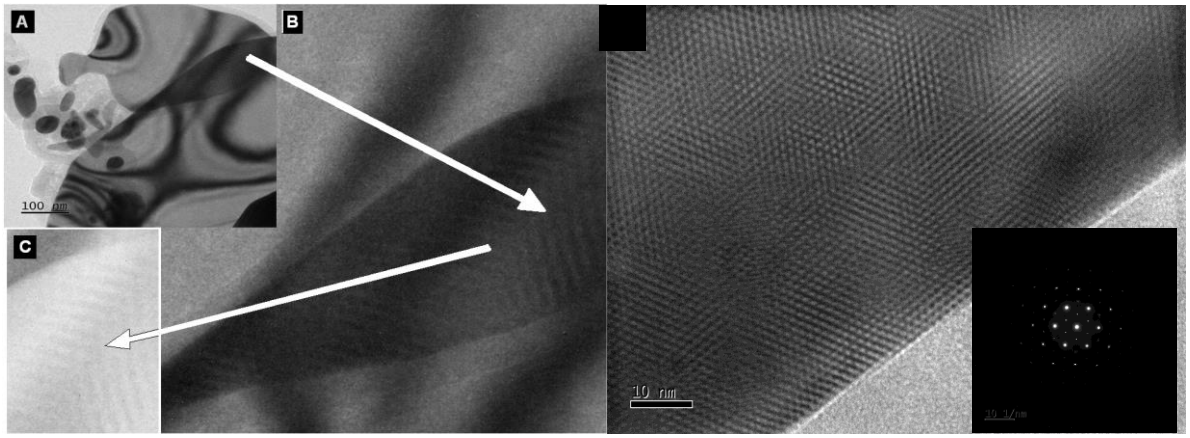

Figure 5. (**A**) TEM image of Phz-Ag particles taken at the initial stage of formation of polymer microcrystals; (**B**) the fragment indicated by the arrow shown at higher magnification; (**C**) the image of the fragment with inverted contrast (the same magnification). (**D**) HRTEM image of a plane of the Phz-Ag crystal and (**E**) its diffraction pattern.

Two sets of stripes are visible in the magnified image of the large particle (Figure 5b) as well as in the same image presented with inverted contrast (Figure 5c). The stripes are oriented at an angle of 120º in relation to each other, which is close to the bond angle inherent to structural units (Phz-Ag). We believe that this structure appeared due to the superposition of the lattices of polymer layers of two crystallites (the Moire patterns). It was not possible to determine the spatial period of the stripes from TEM images since these thin 2D structures are not flat; they can be inhomogeneously deformed or located at different angles to the electron beam.

Figure 5d shows the image of Phz-Ag particles obtained using high-resolution transmission electron microscopy. Spatial periodicity and hexagonal packing of structural elements are present throughout the field. The spatial period is equal to about one nanometer in all directions. The image includes areas with different contrasts; however, the orientation and the ordered arrangement of elements are preserved. Therefore, the presence of contrast cannot be attributed to domains with random orientation. Most likely, this is the effect of the superposition of two or more polymer layers, whose structures differ slightly due to local deformations. The inset shows the selected area electron diffraction pattern Phz-Ag, which confirms the hexagonal symmetry of the structural elements of the material.

Energy dispersive X-ray analysis (EDX) made it possible to carry out the so-called mapping of the Phz-Ag sample at ×10 000 magnification and to visualize the elemental composition of the product (distribution of elements over its surface, Figure 6). The table shows the weight and atomic composition of the product at each point of the spectrum (In, Sn, and P are constituents of the substrate). It can be seen that all the elements included in the synthesized Phz-Ag are present at all points of the studied field. According to the EDX data, the ratio of C, N, and O is somewhat different from the elemental composition of Phz-Ag. This is because EDX is less accurate in quantitative analysis than chemical analytical methods since it relies on specific standards, and its sensitivity to these standards should be considered. The most accurate results can be obtained when determining the contents of heavy elements (in our case, silver).

Silver is also distributed throughout the image. The silver content varies significantly (from 60 to 2 wt.% at different points in the field). The maximum Ag content (63 wt.%) is naturally observed when the electron beam is aimed at a large metal particle. However, the average silver content calculated from the EDX data (23 wt.%) is significantly lower than that

obtained by elemental analysis (63 wt.%). This difference is explained by the fact that EDX does not take into account silver in the ionic form, and only silver metal is registered (which is related to the nature of the standard). According to rough estimates, the content of ionic silver reaches one-third of the total silver amount in the sample (20 wt.% in Phz-Ag).

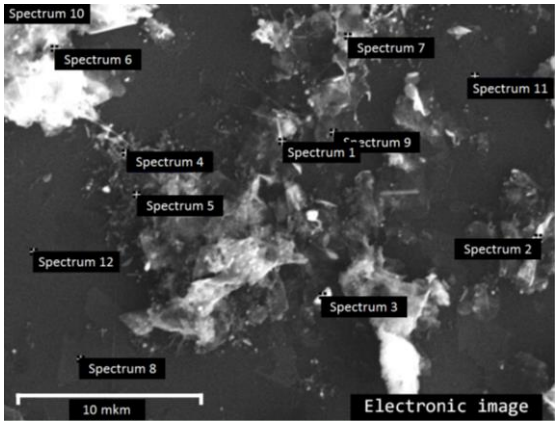

Figure 6. The electronic image of the Phz-Ag sample on conductive ITO substrate.

Table 1. Elemental analysis of the Phz-Ag sample on ITO substrate. Normalized weight/atomic percentages of the product at each point of the spectrum are given (In, Sn, P are contained in the substrate).

Spectrum	C	N	O	Ag	In	Sn	P
№ 1	39/56	28/35	4.7/5.1	25/4	1.50/0.22	1.27/0.18	0.07/0.04
№ 2	45/61	28/32	3.6/3.7	21/3	0.98/0.14	0.32/0.04	0.22/0.11
№ 3	20/49	15/32	0.5/1.0	63/17	1.20/0.31	-0.20/-0.05	-0.01/-0.01
№ 4	46/69	17/23	1.8/2.1	25/4	4.52/0.71	4.00/0.61	0.06/0.04
№ 5	57/70	21/23	5.5/5.0	12/2	1.10/0.14	0.77/0.09	0.33/0.15
№ 6	33/56	22/33	1.8/2.3	38/7	1.91/0.34	1.37/0.24	0.12/0.08
№ 7	42/60	26/32	2.8/3.0	26/4	1.25/0.19	0.43/0.06	0.13/0.07
№ 8	39/62	16/22	8.7/10.2	19/3	6.88/1.13	8.84/1.40	0.14/0.09
№ 9	46/70	14/18	5.8/6.6	21/4	4.94/0.77	5.78/0.87	0.01/0.01
№ 11	42/62	14/18	13.9/15.2	3/1	9.91/1.51	15.10/2.22	-0.12/-0.07
№ 12	58/79	13/15	2.6/2.7	2/0	8.25/1.15	14.72/1.99	0.22/0.11
Average	42/63	19/26	4.7/5.2	23/5	3.86/0.60	4.76/0.70	0.10/0.06
Standard deviation	10/8	5/7	3.8/4.2	16/5	3.25/0.48	5.72/0.82	0.12/0.06
Maximum	58/79	28/35	13.9/15.2	63/17	9.91/1.51	15.10/2.22	0.33/0.15
Minimum	20/50	13/15	0.5/1.0	2.02/0	0.98/0.14	-0.20/-0.05	-0.12/-0.07

3.4. Spectral analysis.

The electronic spectrum of the product (Figure 7 (1)) includes broad overlapping bands in the 200 – 350 nm area and intense absorption starting at 400 nm and extending into the near-IR range. The absorption in the 200 – 280 nm range corresponds to n-π and π-π electronic transitions in benzene rings, and the small individual band with the maximum at 295 nm is attributed to ionic silver ($AgNO_3$) (Figure 7 (3)). The presence of silver nitrate in the resulting product supports the idea of doping Phz-Ag with $AgNO_3$. The peaks corresponding to electronic transitions in individual molecules (aniline and phenazine) lie in the wavelength region below 300 nm [64]; they were not observed in the spectrum of the coordination polymer.

Besides, the spectrum of the product does not contain the peak assigned to the oxidized form of phenazine (Figure 7 (2)), which is the intermediate product of Phz-Ag synthesis.

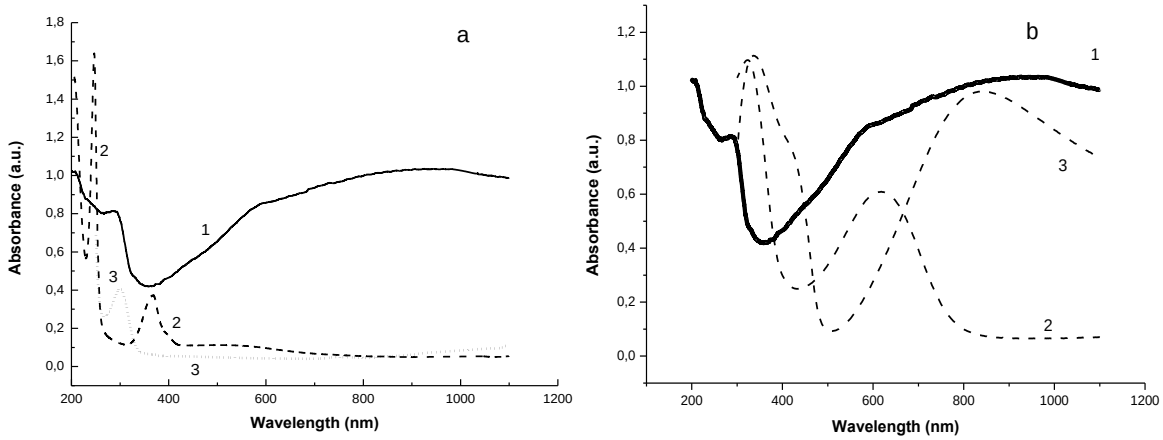

Figure 7. (**a**) Electronic absorption spectra samples: (**1**) Phz-Ag; (**2**) intermediate product of the synthesis (phenazine in oxidized form); (**3**) aqueous solution of $AgNO_3$. Samples were dispersed or dissolved in water at pH 7. **Figure 7(b)** (**1**) aqueous dispersion of Phz-Ag at pH 7; (**2**) electronic absorption spectra of the aqueous dispersion of polyaniline at pH 7 and (**3**) at pH 1.

The region above 400 nm (where the widest absorption band of Phz-Ag is observed) is usually associated with a developed conjugation system containing charge carriers. Similar broad absorption bands were observed in the spectra of electrically conductive conjugated polymers (polyaniline, polypyrrole, polythiophene, PEDOT); they are attributed to the excitation of charge carriers (positive polarons) [65,66]. Since the synthesis of Phz-Ag was carried out by oxidative activation of the C – H bond of aniline with silver ions (oxidation potential +0.7 V), it was necessary to check whether the product contains polyaniline (or is completely composed of polyaniline). This polymer is also synthesized by oxidative polymerization of aniline, albeit with the use of stronger oxidizing agents with potentials higher than +1 V [67].

Figure 7b shows electronic spectra of aqueous dispersions of polyaniline taken at different pH values; the spectrum of Phz-Ag aqueous dispersion (pH 7) is presented for comparison. At pH 7, polyaniline shows the absorption band at 600 nm, corresponding to the system with localized charge carriers (this form of polyaniline has low electrical conductivity (10^{-8} S/ cm)). In an acidic medium (pH < 3), polyaniline becomes doped with acid, and its electrical conductivity reaches 10^0 S/cm. The corresponding absorption band widens and shifts toward the long-wave region [68,69]. Although the general pattern of the doped polyaniline spectrum resembles the spectrum of Phz-Ag, some differences can be noted. In the doped polyaniline spectrum, carrier absorption bands begin in the region around 600 nm, and their intensity decreases after 800 nm (as opposed to that of the Phz-Ag band). In addition, spectral characteristics of Phz-Ag do not depend on the medium's acidity, which is, on the contrary, typical of polyaniline [70]. Based on the above studies, it can be concluded that the resulting product contains neither free low molecular weight reagents nor polyaniline. The product is an advanced conjugated structure that differs from polyaniline.

3.5. Conductivity.

Phz-Ag in the form of dry powder can be easily compressed; durable pellets were obtained already at a pressure of 100 kg/cm^2. The value of the specific electrical conductivity

of the material at room temperature exceeds 10^3 S/cm. Measurements involving multiple samples give values ranging from 1200 S/cm to 7160 S/cm depending on the used pressure. High values of electrical conductivity of the samples are primarily associated with the presence of silver metal and the formation of percolation paths over the metal dispersed in the polymer matrix. However, the reason for the appearance of high conductivity in the material with a relatively low content of silver metal remains unclear. The total mass fraction of silver in Phz-Ag does not exceed 65%; therefore, its volume fraction cannot be higher than 17%. This value represents the theoretical threshold above which we observe the formation of conductive paths for spherical conductor particles homogeneously distributed in a non-conductive matrix. However, it should be taken into account that the real volume fraction of the metal in Phz-Ag is lower since a significant part of the silver exists in the ionic state.

To explain the low percolation threshold, it is necessary to reveal the distinctive pattern of metal distribution in the polymer matrix. The electron microscopy data (Fig. 4 b, 5 a) make it possible to see the "motley color" of polymer plates and the pattern of dark stripes on their surface. It is supposed that the dark deposits are atomic layers of silver metal embedded in the polymer structure. During pressing, the Phz-Ag plates are stacked flat on each other, ensuring good overlapping of these metal strips. Even a small amount of silver metal (2-3 vol.%) creates the strip structure on the polymer layers; therefore, this amount is sufficient to provide a low percolation threshold and high conductivity. Another factor facilitating high conductivity is the extended conjugation system [3,22] formed by phenazine ligands and includes charge carriers in the form of oxidized nitrogen atoms doped with silver nitrate. We will attempt to confirm this hypothesis in the following discussion of the possible structure of Phz-Ag.

3.6. Possible structure of Phz-Ag.

The results of the investigations described above enabled us to propose the structure of the synthesized CP. The composition of the CP corresponds to $[Ag_{3.5}(Phz^{+}NO_3^{-})]$, where the main structural element is the oxidized phenazine ligand. It is believed that in Phz-Ag, flat phenazine ligands are butt-ended (like graphene) and form the polymer layer (2D conjugation system). A part of nitrogen atoms embedded in the aromatic structure is oxidized and forms a positive charge carrier (cation-radical). This structure can act as an organic conductor since it possesses both transport paths (conjugation system) and charge carriers (cation-radicals). It can be assumed that $AgNO_3$ molecules (considered bridges between organic ligands) are localized between oxidized and neutral nitrogen atoms of different molecules. Nitrate anions stabilize a positive charge carrier, while Ag^+ ions interact with lone electron pairs of neutral nitrogen atoms. The hypothetical structure of the Phz-Ag layer is presented in Figure 8. The scheme does not show the guest element (silver metal).

The plate-shaped Phz-Ag particle visible in TEM images consists of several polymer layers bound by π-π-electron interactions. This structure can provide electron tunneling in the direction perpendicular to the particle plane and strongly facilitates the transport of charge carriers between individual plates. The metal-organic matrix has a low density (2.2 g/cm^3), which indicates the presence of large free interatomic space; thus, guest elements can be introduced into the matrix. Metallic silver is present as a guest element in Phz-Ag in the form of spherical nanoparticles or stripes embedded in the polymer layer. Metallic silver helps maintain such a high Phz-Ag electrical conductivity (due to the specific distribution of the metal on the polymer surface). It is presumed that the organic conductor also contributes to the conductivity of the Phz-Ag coordination polymer.

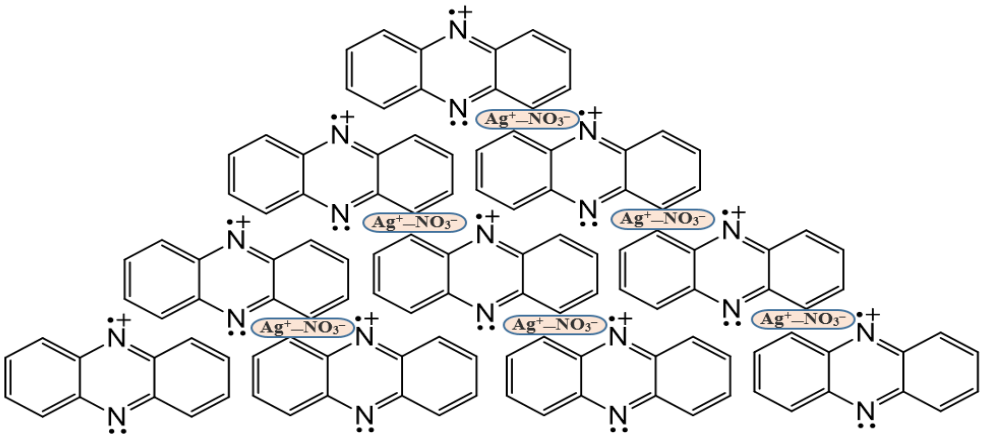

Figure 8. Possible structure of Phz-Ag. Oxidized phenazine ligands doped with $AgNO_3$ molecules form a 2D conjugation system.

4. Conclusions

One-pot synthesis in the solution obtained a new coordination polymer based on phenazine ligands and silver in both ionic and metallic states. The peculiarity of the synthesis was that it included a preliminary stage of phenazine production by oxidative dimerization of aniline. At the same time, the formation of metallic silver as a by-product of this stage proceeded. The reaction ended with the self-organization of phenazine ligands and excess $AgNO_3$ into a coordination polymer with a conjugated structure saturated with the guest element – metallic silver nanoforms. The parallel course of the above reactions during one-pot synthesis leads to the formation of a highly organized CP nanostructure, where the metal is evenly distributed on the surface of the polymer layers.

The polymer has a 2D crystal structure composed of micron-sized planar particles about 10 nm thick. In a dry state, the material is a yellow-brown powder that can be easily dispersed in water. The Phz-Ag particles consist of several polymer layers that are bound by π-π-electron interactions. The polymer composition corresponds to the formula $[Ag_{3.5} (Phz^{+} NO_3^{-})]$, where phenazine ligands exist in the oxidized form and are doped with Ag^{+} and NO_3^{-} ions. Metallic silver (guest element) distributed over the surface of the polymer and between polymer layers imparts high electrical conductivity to Phz-Ag (above 1000 S/cm). The Phz-Ag can be pressed and used as electrode material in contact with human skin. Such electrodes are biocompatible, contain silver in both metallic and ionic states, and can serve as an alternative to the Ag/AgCl electrodes commonly used for encephalography.

Funding

This research did not receive any specific grant from funding agencies in the public, commercial, or not-for-profit sectors.

Conflicts of Interest

The authors declare no conflict of interest.

References

1. Tran, M.; Kline, K.; Qin, Y.; Shen, Y.; Green, M.D.; Tongaya S. 2D coordination polymers: Design guidelines and materials perspective. *Appl. Phys.* **2019**, *6*, 041311, https://doi.org/10.1063/1.5110895.

2. Rowsell, J. L. C.; Yaghi, O. M. Metal-Organic Frameworks: A New Class of Porous Materials. *Microporous and Mesoporous Materials* **2004**, *73*, 3−14, https://doi.org/10.1016/j.micromeso.2004.03.034.
3. Lilia, S.X.; Skorupskii, G.; Dinca. M.; Electrically Conductive Metal−Organic Frameworks. *Chem. Rev*. **2020**, *120*, 8536−8580, https://dx.doi.org/10.1021/acs.chemrev.9b00766.
4. Kung, C.-W.; Otake, K.; Buru, C. T.; Goswami, S.; Cui, Y.; Hupp, J. T.; Spokoyny, A. M.; Farha, O. K. Increased Electrical Conductivity in a Mesoporous Metal−Organic Framework Featuring Metallacarboranes Guests. *J. Am. Chem. Soc.* **2018**, *140*, 3871−3875, https://doi.org/10.1021/jacs.8b00605.
5. Li, W.; Sun, L.; Qi, J.; Jarillo-Herrero, P.; Dinc, M.; Li, J. High temperature ferromagnetism in π-conjugated two-dimensional metal–organic frameworks. *Chem. Sci*. **2017**, *8*, 2859, https://doi.org/10.1039/c6sc05080h.
6. Furukawa, H.; Cordova, K. E.; O'Keeffe, M.; Yaghi, O. M. The Chemistry and Applications of Metal-Organic Frameworks. *Science* **2013**, *341*, 1230444, https://doi.org/10.1126/science.1230444.
7. Sakamoto, R., Takada, K.; Pal, T.; Maeda, H.; Kambe, T.; Nishihara, H. Coordination nanosheets (CONASHs): strategies, structures and functions. *Chem. Commun*. **2017**, *53*, 5781, https://doi.org/10.1039/C7CC00810D.
8. Zhan, G.; Zeng, H.C. Synthesis and Functionalization of Oriented Metal–Organic-Framework Nanosheets: Toward a Series of 2D Catalysts. *Adv. Functional Mater* **2016**, *26*, 3268-3281, https://doi.org/10.1002/adfm.201505380.
9. Yan, R.; Zhao, Y.; Yang, H.; Kang, X.J.; Wang, C.; Wen, L-L.; Lu, Z-D. Ultrasmall Au Nanoparticles Embedded in 2D Mixed-Ligand Metal–Organic Framework Nanosheets Exhibiting Highly Efficient and Size-Selective Catalysis. *Adv. Functional Mater*. **2018**, *28*, 1802021, https://doi.org/10.1002/adfm.201802021.
10. Herm, Z. R.; Bloch, E. D.; Long, J. R. Hydrocarbon Separations in Metal-Organic Frameworks. *Chem. Mater*. **2014**, *26*, 323−338, https://doi.org/10.1021/cm402897c.
11. Quoc, B., Vargun, E.; Fei, H.; Cheng, Q.; Bubulinca, C.; Mouc˘ ka, R.; Sapurina, I.; Trong, T.D.; Kazantseva, N.E.; Saha, P. Effect of PANI and PPy on Electrochemical Performance of rGO/ZnMn2O4 Aerogels as Electrodes for Supercapacitors. *Journal of Electronic Materials, The Minerals, Metals & Materials Society* **2020**, *49*, 4697-4706, https://doi.org/10.1007/s11664-020-08198-4.
12. Zhao, X.; Zheng, Y.; Dai, H.; Yang, J.; Chen, Q.; Zhou, J.; Sun, G. Wet-Chemistry: A Useful Tool for Deriving Metal–Organic Frameworks toward Supercapacitors and Secondary Batteries. *Advanced Materials Interfaces* **2022**, *9*, 13, https://doi.org/10.1002/admi.202102595.
13. Noro, S.; Chang, H.-C.; Takenobu, T.; Murayama, Y.; Kanbara, T.; Aoyama, T.; Sassa, T.; Wada, T.; Tanaka, D.; Kitagawa, S.; et al. Metal−Organic Thin-Film Transistor (MOTFT) Based on a Bis(o-Diiminobenzosemiquinonate) Nickel (II) Complex. *J. Am. Chem. Soc*. **2005**, *127*, 10012−10013, https://doi.org/10.1021/ja052663s.
14. Sengupta, A.; Datta, S.; Su, C.; Herng, T.S.; Ding, J.; Vittal, J.J.; Loh, K.P.; Tunable Electrical Conductivity and Magnetic Property of the Two Dimensional Metal Organic Framework [Cu(TPyP)Cu2(O2CCH3)4]. *ACS Appl. Mater. Interfaces* **2016**, *8*, 16154, https://doi.org/10.1021/acsami.6b03073.
15. Chaudhari, A.K.; Kim, H.J.; Han, I.; Tan, J.C. Optochemically Responsive 2D Nanosheets of a 3D Metal–Organic Framework Material. *Adv. Mater.* **2017**, *29*, 1701463, https://doi.org/10.1002/ama.201701463.
16. Wang, X.; Li, C.; Li, Z.; Ma, X.; Wan, C.H.; Deng, Z.; Deng, R.; Peng, X. Near-Infrared-Light emitting diode driven white light Emission: Upconversion nanoparticles decorated Metal-Organic Frame-works thin film. *Chemical Engineering Journal* **2021,** *409*, 128220, https://doi.org/10.1016/j.cej.2020.128220.
17. Xu, Y. H., Nagai, A.; Jiang, D. L. Core-shell conjugated microporous polymers: a new strategy for exploring color-tunable and -controllable light emissions. *Chem. Comm*. **2013**, *49*, 1591–1593, https://doi.org/10.1039/C2CC38211C.
18. Aubrey, M. L.; Kapelewski, M. T.; Melville, J. F.; Oktawiec, J.; Presti, D.; Gagliardi, L.; Long, J. R. Chemiresistive Detection of Gaseous Hydrocarbons and Interrogation of Charge Transport in Cu[Ni(2,3-Pyrazinedithiolate)2] by Gas Adsorption. *J. Am. Chem. Soc.* **2019**, *141*, 5005−5013, https://doi.org/10.1021/jacs.9b00654.
19. Lee, K.; Park, J.; Song, I.; Yoon, S.M. The Magnetism of Metal–Organic Frameworks for Spintronics. *Bulletin of the Korean Chemical Society* **2021**, *42*, 1170-1183, https://doi.org/10.1002/bkcs.12362.
20. Guan, N.-B.; Zhang, B.; Wang, T-J. Two Cu(II) and Co(II) coordination polymers: Magnetic properties and nutritional support for breast cancer patients by increasing the intestinal epithelial cell microvilli absorption. *Journal of Solid-State Chemistry* **2021**, *297*, 122067, https://doi.org/10.1016/j.jssc.2021.122067.

21. Branzea, D.G.; Madalan, A.M.; Ciattini, S.; Avarvari, N.; Caneschi, A.; Andruh, M. New heterometallic coordination polymers constructed from 3d–3d′ binuclear nodes. *New J. Chem.*, **2010**, *34*, 2479-2490, https://doi.org/10.1039/C0NJ00238K.
22. Robertson, N.; Cronin, L. Metal Bis-1,2-Dithiolene Complexes in Conducting or Magnetic Crystalline Assemblies. Coord. Chem. Rev. 2002, 227, 93−127. https://doi.org/10.1016/S0010-8545(01)00457-X
23. Lustig, W.P.; Coord, J.L. Luminescent metal–organic frameworks and coordination polymers as alternative phosphors for energy efficient lighting devices. *Chem. Rev.* **2018**, *373*, 116-147, https://doi.org/10.1016/j.ccr.2017.09.017.
24. Jiang, S.; Wang, J.; Zhu, Z.; Shan, S.; Mao, Y.; Zhang, X.; Pei, X.; Huang, C.; Wan, Q. The synthesis of nano bio-MOF-1 with a systematic evaluation on the biosafety and biocompatibility. *Microporous and Mesoporous Materials* **2022**, *334*, 111773, https://doi.org/10.1016/j.micromeso.2022.111773.
25. Rabiee, N.; Atarod, M.; Tavakolizadeh, M.; Asgari, S.; Rezaei, M.; Akhavan, O.; Pourjavadi, A.; Jouyandeh, M.; Lima, E.C.; Mashhadzadeh, A.H.; Ehsani, A.; Ahmadi, S.; Saeb, M.R. Green metal-organic frameworks (MOFs) for biomedical applications. *Microporous and Mesoporous Materials* **2022**, *335*, 111670, https://doi.org/10.1016/j.micromeso.2021.111670.
26. McKinlay, A.C.; Horcajada, M.P.; Férey, G.; Gref, R.; Serre. C.; BioMOFs: Metal–Organic Frameworks for Biological and Medical Applications **2010**, *49*, 6260-6266, https://doi.org/10.1002/anie.201000048.
27. Palakollu, V.N.; Chen, D.; Tang, J-N.; Wang, L.; Liu, C.Recent advancements in metal-organic frameworks composites based electrochemical (bio)sensors. *Microchimica Acta* **2022**, *189*, https://doi.org/10.1007/s00604-022-05238-0.
28. André, V.; Alves, P.C.; Duarte, M.T. Exploring antibiotics as ligands in metal–organic and hydrogen bonding frameworks: Our novel approach towards enhanced antimicrobial activity (mini-review). *Inorganica Chimica Acta* **2021**, *525*, 120474, https://doi.org/10.1016/j.ica.2021.120474.
29. Malik, P.; Gupta, R.; Ameta, R.K. Unique attributes of metal-organic frameworks in drug delivery. *Metal-Organic Frameworks for Chemical Reactions* **2021**, 389-415, https://doi.org/10.1016/B978-0-12-822099-3.00016-2.
30. Zhou, Z.; Vázquez-González, M.; Willner, I.; Stimuli-responsive metal–organic framework nanoparticles for controlled drug delivery and medical applications. *Chemical Society Reviews* **2021**, *50*, 4541, https://doi.org/10.1039/D0CS01030H.
31. Yang, J.; Yang, Y-W. Diagnosis Employing MOFs (Fluorescence, MRI) *Metal-Organic Frameworks in Biomedical and Environmental Field* **2021**, 433-455, https://doi.org/10.1007/978-3-030-63380-6.
32. Li, X.; Zhang, Y.; Liu, G.K.; Luo, Z.; Xue, Y.; Liu, M. Recent progress in the applications of gold-based nanoparticles towards tumor-targeted imaging and therapy. *RSC Advances* **2022**, *12*, 7635, https://doi.org/10.1039/D2RA00566B.
33. Wang, Y.; Shi, L.; Wu, W.; Qi, G.; Zhu, X.; Liu, B. Tumor-Activated Photosensitization and Size Transformation of Nanodrugs. *Advanced Functional Materials* **2021,** *31*, 2010241, https://doi.org/10.1002/adfm.202010241.
34. Singh, S.; Aldawsari, H.M.; Alam, A.; Alqarni, M.H.S.; Ranjan, S.; Kesharwani, P. Synthesis and antimicrobial activity of vancomycin–conjugated zinc coordination polymer nanoparticles against methicillin-resistant staphylococcus aureus. *Journal of Drug Delivery Science and Technology* **2022**, *70*, 103255, https://doi.org/10.1016/j.jddst.2022.103255.
35. Claudio Pettinari, Riccardo Pettinari, Corrado Di Nicola, Alessia Tombesi, Stefania Scuri, Fabio Marchetti, Antimicrobial MOFs. *Coordination Chemistry Reviews* **2021**, *446*, 214121, https://doi.org/10.1016/j.ccr.2021.214121.
36. Li, R.; Chen, T.; Pan, X. Metal–Organic-Framework-Based Materials for Antimicrobial Applications. *ACS Nano* **2021**, *15*, 3808, https://doi.org/10.1021/acsnano.0c09617.
37. Zhang, S.; Ma, X.; Yu, H.; Lu, X.; Liu, J.; Zhang, L.; Wang, G.; Ye, J.; Ning, G. Silver(i) metal–organic framework-embedded polylactic acid electrospun fibrous membranes for efficient inhibition of bacteria. *Dalton Transactions* **2022**, *51*, 6673, https://doi.org/10.1039/D1DT04234C.
38. Yue, T.; Jing, Y.; Tan, L.; Xue, R. Co(II)-coordination polymer: treatment and testing values on calculus of ureter by inhibiting the growth of urinary tract pathogens. *Inorganic and Nano-Metal Chemistry* **2021**, *52*, 693, https://doi.org/10.1080/24701556.2021.1952235.
39. Veerana, M.; Kim, H-C.; Mitra, S.; Adhikari, B.C.; Park, G.; Huh, S; Kim, S-J.; Kim, Y. Analysis of the effects of Cu-MOFs on fungal cell inactivation. *RSC Advances* **2021**, 11, 1057, https://doi.org/10.1039/D0RA08743B.

40. Guan, N-B.; Zhang, B.; Wang, T-J. Two Cu(II) and Co(II) coordination polymers: Magnetic properties and nutritional support for breast cancer patients by increasing the intestinal epithelial cell microvilli absorption. *Journal of Solid-State Chemistry* **2021**, *297*, 122067, https://doi.org/10.1016/j.jssc.
41. Bieniek, A.; Terzyk, A.P.; Wiśniewski, M.; Roszek, K.; Kowalczyk, P.; Sarkisov, L.; Keskin, S.; Kaneko, K. MOF materials as therapeutic agents, drug carriers, imaging agents and biosensors in cancer biomedicine: Recent advances and perspectives. *Progress in Materials Science* **2021**, *117*, 743, https://doi.org/10.1016/j.pmatsci.2020.100743.
42. Kenawy, S.H.; Khalil, A.M. Advanced ceramics and relevant polymers for environmental and biomedical applications. *Biointerface Research in Applied Chemistry* **2020**, *10*, 5747-5754, https://doi.org/10.33263/briac104.747754.
43. Dou, J. H.; Sun, L.; Ge, Y.; Li, W.; Hendon, C. H.; Li, J.; Gul, S.; Yano, J.; Stach, E. A.; Dinca, M. Signature of Metallic Behavior in˘the Metal-Organic Frameworks M3(Hexaiminobenzene)2 (M = Ni, Cu). *J. Am. Chem. Soc*. **2017**, *139*, 13608−13611, https://doi.org/10.1021/jacs.7b07234.
44. Huang, X.; Sheng, P.; Tu, Z.; Zhang, F.; Wang, J.; Geng, H.; Zou, Y.; Di, C.; Yi, Y.; Sun, Y.; Xu, W.; Zhu, D. A two-dimensional p–d conjugated coordination polymer with extremely high electrical conductivity and ambipolar transport behavior. *NATURE COMMUNICATIONS* **2015**, *6*, 7408, https://doi.org/10.1038/ncomms8408.
45. Liu, X.-H., Guan, C.-Z., Wang, D. & Wan, L.-J. Graphene-like single-layered covalent organic frameworks: synthesis strategies and application prospects. *Adv. Mater*. **2014**, *26*, 6912–6920, https://doi.org/10.1002/adma.201305317.
46. Day, R. W.; Bediako, D. K.; Rezaee, M.; Parent, L. R.; Skorupskii, G.; Arguilla, M. Q.; Hendon, C. H.; Stassen, I.; Gianneschi, N.; Kim, P.; et al. Single Crystals of Electrically Conductive 2D MOFs: Structural and Electrical Transport Properties. *ACS Cent. Sci.* **2019**, *5*, 1959−1964, https://doi.org/10.1021/acscentsci.9b01006.
47. Wang, Z.F.; Su, N.; Liu, F.; Prediction of a Two-Dimensional Organic Topological Insulator. *Nano Lett*. **2013**, *13*, 2842-2845, https://doi.org/10.1021/nl401147u.
48. Dar1, D.; Thomashow, L.S.; Weller, D.M.; Newman, D.K. Global landscape of phenazine biosynthesis and biodegradation reveals species-specific colonization patterns in agricultural soils and crop microbiomese. *Life* **2020**, *9*, e59726, https://doi.org/10.7554/eLife.59726.
49. Cornell, W.C.; Zhang, Y.; Bendebury, A.; Hartel, A.J.W.; Shepard, K.L.; Dietrich. L.E.P. Phenazine oxidation by a distal electrode modulates biofilm morphogenesis. *Biofilm* **2020**, *2*, 100025, https://doi.org/10.1016/j.bioflm.2020.100025.
50. Balaji, S.; Shanmugam, V.K. Enhanced Antibiofilm Activity of Endophytic Bacteria Mediated Zirconium Nanoparticles. *Biointerface Research in Applied Chemistry* **2022**, *12*, 74–82, https://doi.org/10.33263/BRIAC121.074082.
51. Fadlilah, D.R.; Endarko, E.; Ratnasari, A.; Hozairi, H.; Yusop, Z.; Syafiuddin A. Enhancement of antibacterial properties of various polymers functionalized with silver nanoparticles. *Biointerface Research in Applied Chemistry* **2020**, *10*, 5592-5598, https://doi.org/10.33263/BRIAC0103.592598.
52. Hamzah, H.; Nabilah, T.U.; Yudhawan, I.; Siregar, K.A.A.K.; Sammulia, S.F.; Fitriani. Investigation and Development of Anti Polymicrobial Biofilm from Several Essential Oils: A Review. *Biointerface Research in Applied Chemistry* **2023**, *13*, 103, https://doi.org/10.33263/BRIAC132.103.
53. Chen, I.F.; Lu, C.F.; Su, W.F. Highly conductive 2D metal–organic framework thin film fabricated by liquid–liquid interfacial reaction using one-pot-synthesized benzenehexathiol. *Langmuir* **2018**, *34*, 15754-15762, https://doi.org/10.1021/acs.langmuir.8b03938.
54. Butova, V.V.; Soldatov, M.A.; Guda, A.A.; Lomachenko, K.A.; Lamberti, C. Metal-organic frameworks: structure, properties, methods of synthesis and characterization. *Russ. Chem. Rev.* **2016**, *85*, 280-307, https://doi.org/10.1070/RCR4554.
55. Lee, Y.-R.; Kim, J.; Ahn, W.S. Synthesis of metal-organic frameworks: A mini review. *Korean J. Chem. Eng*. **2013**, *30*, 1667-1680, https://doi.org/10.1007/s11814-013-0140-6.
56. Seth, K.; Roy, S.R.; Chakraborti, A.K. A Synchronous Double C-N Bond Formation via C-H Activation as a Novel Synthetic Route to Phenazine. *Chem. Comm*. **2016**, *52*, 922-925, https://doi.org/10.1039/C5CC08640J.
57. Wang, T.; Chen, S.; Shao, A.; Gao, M.; Huang, Y.; Lei, A. Silver-Mediated Selective Oxidative Cross-Coupling between C−H/ P−H: A Strategy to Construct Alkynyl(diaryl)phosphine Oxide. *Org. Lett*. **2015**, *17*,118-121, https://doi.org/10.1021/ol503341t.

58. Fujiwara, Y.; Domingo, V.; Seiple, I.B.; Gianatassio, R.; Bel, M.D.; Baran. P.S. Practical C-H Functionalization of Quinones with Boronic Acids. *J. Am. Chem. Soc*. **2011**, *133*, 3292–3295, https://dx.doi.org/10.1021/ja111152z.
59. Shi, G.; Shao, C.; Pan, S.; Yu, J.; Zhang, Y. Silver-Catalyzed C−H Trifluoromethylation of Arenes Using Trifluoroacetic Acid as the Trifluoromethylating Reagent. *Org. Lett.* **2015**, *17*, 38–41, https://doi.org/10.1021/ol503189j.
60. Girard, S.A.; Knauber, T.; Li, C.J. The Cross-Dehydrogenative Coupling of C_{sp^3}-H Bonds: A Versatile Strategy for C-C Bond Formations. *Angew. Chem. Int. Ed*. **2014**, *53*, 74, https://doi.org/10.1002/anie.201304268.
61. Alberico, D.; Scott M.E.; Lautens, M. Aryl-aryl bond formation by transition-metal-catalyzed direct arylation. *Chem. Rev*. **200**7, *107*, 174; https://doi.org/10.1021/cr0509760.
62. Cho, S.H.; Kim, Y.J.; Kwak, J.; Chang, S. Recent advances in the transition metal-catalyzed twofold oxidative C–H bond activation strategy for C–C and C–N bond formation. *Chem. Soc. Rev*. **2011**, *40*, 5068, https://doi.org/10.1039/C1CS15082K.
63. Kompan, M. E.; Klimov, V. A.; Rozanov V. V.; Evstrapov A. A. Self-Organizing Structure in Platinum Films on a Nafion Type Polymer Membrane. *Technical Physics Letters* **2009**, *35*, 234-236, https://doi.org/10.1134/S1063785009030122.
64. Stern, E.S.; Timmons, C.J. Gillam and Stern's introduction to electronic absorption spectroscopy in organic chemistry. *Electronic Absorption Spectroscopy in Organic Chemistry*, Edward Arnold Publishers. Ltd., London **1970**, 113, 6 ISBN: 0713122676
65. Houze, E., Nechtschein, M., Pron A. Fixed−spin−induced ESR linewidth and polaron mobility in conducting polymers. *Physical Review B*. **1997**, *56*, 12263−12267, https://doi.org/10.1103/PHYSREVB.56.12263.
66. Jozefowicz, M.E.; Laversanne, R.; Javadi, H.H.S.; Epstein, A.J.; Pouget, J.P.; Tang, X.; MacDiarmid, A.G. Multiple lattice phases and polaron lattice spinless defect competition in polyaniline. *Phys. Rev. B*. **1989**, *39*, 12958−12961, https://doi.org/10.1103/PhysRevB.39.12958.
67. Sapurina, I.; Shishov, M.A. Oxidative polymerization of aniline: moleceular synthesis of polyaniline and the formation of supramolecular structures, in: Ailton De Souza Gomes (Ed.), *New Polym. Spes. Appl*. **2012**, 251–312. https://doi.org/10.5772/48758.
68. Nekrasov, A.A.; Ivanov, F.V.; Vannikov A.V. Analysis of structure of polyaniline absorption spectra based on spectroelectrochemical data. *J. Electroanalit Chem* **2000**, *482*, 11−17, https://doi.org/10.1016/S0022-0728(00)00005-X.
69. Thanh-Hai, L.; Yukyung, K.; Hyeonseok Y. Electrical and Electrochemical Properties of Conducting Polymers. *Polymers* **2017**, *9*, 150, https://doi.org/10.3390/polym9040150.
70. Stejskal, J. Colloidal dispersions of conducting polymers. *J. Polymer Materials* **2001**, 18, 225−258.